Flexural Capacity of Corroded Post-tensioned Concrete Beams: Large Scale Tests and Numerical Simulation

Resistencia a flexión de vigas postensadas de hormigón con corrosión: Ensayos a gran escala y simulación numérica

Antonino Recupero*,[a], **Nino Spinella**[b], **Antonio R. Marí**[c], **Jesús M. Bairán**[d]

[a] *Assistant Professor. Dr. Dept. of Engineering, University of Messina, Italy*
[b] *Dr. Research Fellow, Dept. of Engineering, University of Messina, Italy*
[c] *Prof. Dr. Dept. of Civil and Env. Engineering, Universitat Politècnica de Catalunya, Spain*
[d] *Assistant Prof. Dr. Dept. of Civil and Env. Engineering, Universitat Politècnica de Catalunya, Spain*

ABSTRACT

An experimental campaign was carried out at the University of Messina to study the influence of the tendon corrosion on the response of post-tensioned concrete beams under transversal loads. Six beams were cast in 2006 and subjected to induced corrosion of the tendons by injecting a chemical solution or an acid in some parts of the duct. The results showed that the load bearing capacity was reduced up to 50%, with respect to the tested un-corroded beam. The tests were simulated by means of a non-linear time dependent analysis model, developed at UPC, showing its capacity to capture the effects of corrosion along the time and to estimate the degree of corrosion.

©2022 Hormigón y Acero, the journal of the Spanish Association of Structural Engineering (ACHE). Published by Cinter Divulgación Técnica S.L. This is an open-access article distributed under the terms of the Creative Commons (CC BY-NC-ND 4.0) License

KEYWORDS: Post-tensioned, concrete, beam, corrosion, tests, strength, non-linear analysis.

RESUMEN

En la Universidad de Messina se llevó a cabo una campaña de ensayos sobre para conocer los efectos de la corrosión sobre la respuesta estructural de vigas postensadas bajo cargas transversales. En 2006 se construyeron 6 vigas que se sometieron a corrosión inducida de los cordones, mediante inyección de una solución química o ácido en partes de las vainas. Los ensayos bajo carga mostraron una reducción de hasta el 50% de la capacidad portante. Los ensayos fueron simulados con buena aproximación mediante un modelo de análisis no lineal en el tiempo desarrollado en la UPC, mostrando la capacidad del mismo para captar los efectos del deterioro del acero y el grado de corrosión a lo largo del tiempo.

©2022 Hormigón y Acero, la revista de la Asociación Española de Ingeniería Estructural (ACHE). Publicado por Cinter Divulgación Técnica S.L. Este es un artículo de acceso abierto distribuido bajo los términos de la licencia de uso Creative Commons (CC BY-NC-ND 4.0)

PALABRAS CLAVE: Postensado, hormigón, viga, corrosión, ensayo, resistencia, análisis no lineal .

1.
INTRODUCTION

The corrosion of steel reinforcements in concrete is a long-standing a global problem that has caused widespread damage to concrete structures [1]. Therefore, research on the influence of steel corrosion on the global behavior of concrete structures has been both intensive and extensive in the past few decades [2,3]. However, studies have focused more on reinforced concrete (RC) structures than on prestressed concrete (PC) structures, even though PC structures have been used in many constructions and are increasingly being used in new constructions that are particularly vulnerable to steel corrosion [4].

---

* Persona de contacto / *Corresponding author*:
Correo-e / *e-mail*: antonino.recupero@unime.it (Antonino Recupero).

Since their first uses, the PC elements, especially when placed in an aggressive environment, showed a certain degree of vulnerability. The tendons are prone to the corrosion in a faster way than plain rebar, with impacts in terms of efficiency and durability of whole structure. Moreover, the structures involved in corrosion phenomena were mainly exposed to severe environmental conditions (i.e. bridge, external part of building).

In PC structures, the high stress level in the tendons radically modifies the steel corrosion process. The stress corrosion is characterized by the coupling between the conventional corrosion (pitting attacks in chloride environment) and the steel micro-cracking, the latter induced by the high stress level and hydrogen embrittlement [5]. Contestually, for a low corrosion level of tendon and under normal service loading, the steel micro-cracking can lead to the brittle failure. An example of PC structure failure is the Santo Stefano bridge, built in 1954 and designed by Professor Riccardo Morandi, along the coast of the Mediterranean Sea in Sicily. This post-tensioned bridge suddenly collapsed on 1999 without any warning. The main cause of collapse was the uniform corrosion of tendons due to the non-correct injection of the ducts [6].

However, studies regarding the structural response of PC structures affected by corrosion are still rather limited, if compared to the literature about corroded RC elements [7–9]. In addition, most of the studies are focused to the non-destructive monitoring of PC members, to assess the damage evolution due to corrosion phenomena [10,11].

In this scenario, this work presents the experimental and numerical results of a research project about the influence of tendon corrosion on the performances of PC beams.

In 2006, a set of PC beams was casted at the University of Messina Laboratory. Some defects were artificially created along part of the tendon and the specimens were stored in the basement of the lab building. After twelve years, a destructive test campaign was carried out to investigated the degradation of the load bearing capacity of six beams due to the corrosion evolution.

The experimental results, in terms of crack pattern and load-deflection response, are reported and commented. Moreover, a non-linear time dependent analysis model has been developed at Universitat Politècnica de Catalunya (UPC), and it is used to reproduce the effects of corrosion along the time and also to estimate the degree of corrosion.

2.
DESCRIPTION OF THE EXPERIMENTAL CAMPAIGN

The PC specimens had a rectangular shape (400×250 mm) and a total length of 6 300 mm. Prestressing was carried out using 4 tendons of 7-wire 0.6" strands, and steel with an ultimate tension capacity of f_{ys} = 1860 MPa was used. The cable was placed along the centroid axis (figura 1). The longitudinal reinforcement was achieved with $2\phi18$ both at top and bottom of the cross-section. The transverse reinforcement was realized with closed stirrups $\phi8/100$ mm, except for a closest spacing (80 mm) at the ends of the beam and for a transfer length of

800 mm (figura 1). The FeB44k steel rebar was used, with a minimum yield strength of 430 MPa.

Figure 1. Reinforcement setup.

The concrete compressive strength was experimentally evaluated as f_{cm} = 69.7 MPa.

Each tendon was tensioned by a total tension force of 756 kN. For T2 beam, half of maximum tension force was applied (378 kN) with the aim of simulate a cable tension loss.

The others beams were damaged making one or more holes along the beam length and introducing a chemical solution or an acid to locally corrode the tendons. The artificial defects should simulate the imperfect injection of the ducts.

All specimens were designed to achieve a bending failure. The shear span-effective depth ratio (*a/d*) was set more than 10, and the longitudinal reinforcement was calculated taken into account the bending moment at Ultimate Limit State (ULS).

The test setup is represented in figure 2. A three points test was performed by using a pneumatic actuator having a capacity of 1000 kN and a maximum stroke of 700mm was used. Two steel plates, with two cylinders interposed, and a rubber layer over the concrete surface were used to avoid a local failure under the point load.
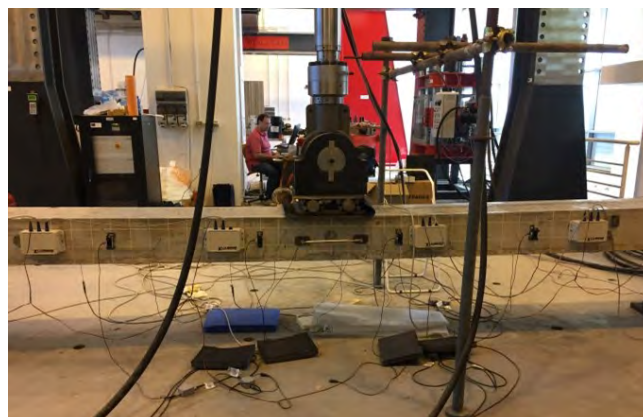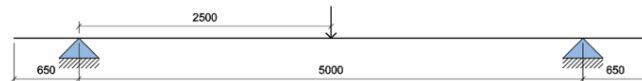

Figure 2. Test setup.

3.
TESTS RESULTS

The specimens subjected to transversal load have been identified as T1, T2, T3a, T4a, T6a and T6b. All six tests have been performed by loading and unloading the beam at increasing load levels for beam T1 (load control), and at increasing displacement levels for the other beams (displacement control): T2, T3a, T4a, T6a and T6b, respectively.

3.1 Beam T1

The beam T1 was without any defect. It was a benchmark specimen with a prestress of tendon equal to target tensile strength (756 kN). Unlike the other beams, this test was performed under force control. Six loading cycles were executed at the following load levels: 25, 50, 75, 100, 130 and 150 kN, respectively.

The response behavior was almost linear until the load level of 100 kN. Then, a stiffness decay was observed, with a soft slope of the curve. The cycle at 130 kN allowed to achieve the maximum load bearing capacity of the beam, and a fast drop of the beam at the mid-span was occurred.

In figure 3, the crack pattern at failure of the region under the load point is reported. It is typical of the bending failure. The top region of the beam has been characterized by crushing of concrete in compression, which has led to the failure.

Figure 3. Crack pattern at failure of beam T1.

3.2. Beam T2

Also the beam T2 was without any defect. However, to simulate a loss of prestressing force, the tendon was prestressed at the 45% of allowable tensile strength.

This test this test, together with all the others, has been performed under displacement control. In this case, seven cycles have been performed at different displacement levels: 10, 20, 40, 60, 80, 100, 120 and 150 mm, respectively.

The response behavior has been almost linear until the imposed displacement of 60mm. At the corresponding load level (about 75 kN), an evident cracking and a stiffness decay has been observed. The cycle at 120 mm allowed to achieve the maximum load bearing capacity of the beam of about 107 kN, then the wide cracking of the plastic hinge region, under the point load, has been also characterized by a softening of the load-displacement curve.
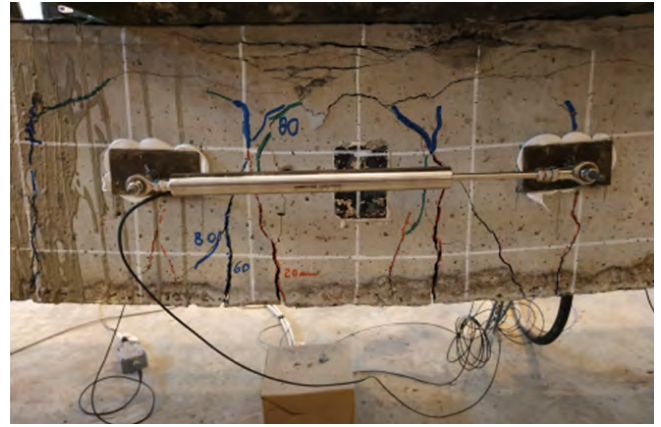

Figure 4. Crack pattern at failure of beam T2.

3.3. Beam T3a

The beam T3a was damaged with a hole inside of the duct at 1/2 of the beam length. A chemical solution was injected in the small tank, 100 mm long, to cause a localized corrosion of the tendon. The test was performed under displacement control, and seven cycles were executed at the following displacement levels: 10, 20, 40, 60, 80, 100 and 140 mm.

The response behavior has been also linear until a maximum load of less than 60 kN, see figure 5.

Figure 5. Crack pattern at failure of beam T3a.

It is almost half of the bearing load achieved by the T1 beam. At the fourth cycle the maximum load bearing capacity of the beam (about 60 kN) has been recorded. The force peak has been followed by a load abruptly decay, and a typical noise of steel breaking has been heard. Probably a strand broke or frayed, in fact the next cycles have been characterized by both lower stiffness and load, with subsequent drops of force. The corrosion in the middle of the tendon has drastically changed the capacity of the beam.

3.4. Beam T4a

This specimen was damaged with a hole inside of the duct at 1/4 of the beam length. A chemical solution was injected in the small tank, 100 mm long, to cause a localized corrosion of the tendon.

The test has been performed under displacement control, and six cycles have been carried out: 10, 20, 40, 80, 100 and 200 mm, respectively.

The response behavior has been almost linear until a load less than 50 kN. At the fourth cycle, the stiffness decay, and the load-displacement curve showed a new branch with different slope. The last cycle has allowed to achieve the maximum load bearing capacity of the beam (more than 60 kN), followed by two subsequent drops of force.

Figura 6. Crack pattern at failure of beam T4a.

3.5. Beam T6a

The beam T6a was prestressed with an un-bonded tendon and, then, the duct was filled with grease injections at 1/6, 1/2 and 5/6 of the beam length, respectively. In the empty parts of the duct, a mould was introduced to cause a spreading corrosion.

The test has been carried out under displacement control, and height cycles have been performed by applying height displacement levels: 10, 20, 40, 60, 80, 100, 120 and 150 mm, respectively.

The response behavior has been almost linear until a load less than 100 kN. It is a smaller value than the same load recorded for the T1 beam.

At the fourth cycle, the stiffness has decayed, and the load-displacement curve showed a new ascending branch with a different slope. Then, at the sixth cycle (100 mm), the maximum load bearing capacity of the beam (about 120 kN) has been reached.
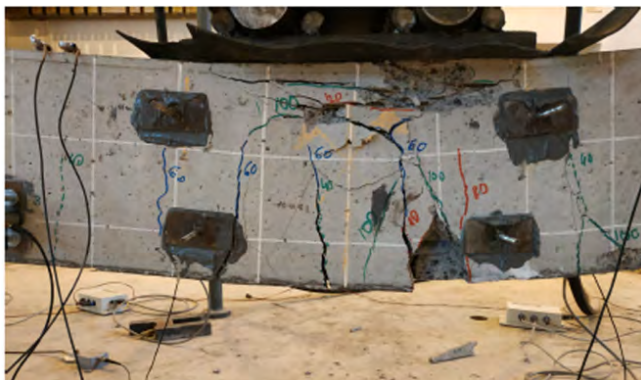

Figura 7. Crack pattern at failure of beam T6a.

3.6. Beam T6b

The beam T6b was a companion specimen of T6a, but it was artificially damaged by introducing a different kind of mould family.

The experimental test has been performed under displacement control, and height cycles have been performed: 10, 20, 40, 60, 80, 100, 150 and 200 mm, respectively.

As for the beam T6a, the load-deflection curve has been almost linear until a load less than 100 kN. At the sixth cycle, the maximum load bearing capacity of the beam (about 115 kN) has been reached.

The experimental tests on the T6 beams allowed to record a load bearing capacity less than T1 beam, but still comparable. The un-bonded prestressing system adopted in these cases has been less prone to the damaging-corrosion action. Moreover, the induced corrosion has been widespread along the tendon. The investigation on the cables, that will be performed at the end of the first phase of the test campaign, should be provided interesting information about the real corrosion condition of the tendons.
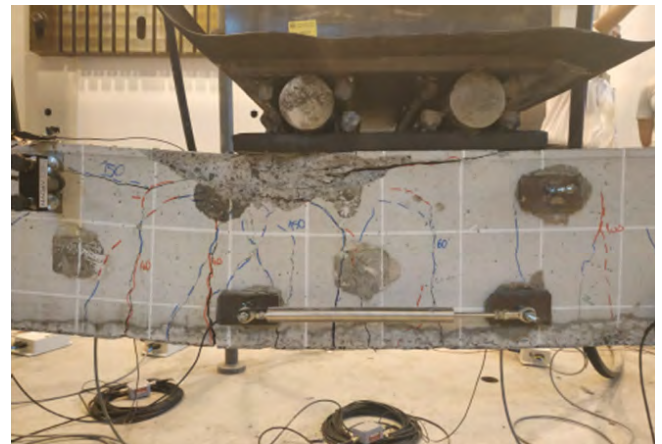

Figure 8. Crack pattern at failure of beam T6b.

4.
DESCRIPTION OF THE NUMERICAL MODEL

The model is based on the displacement formulation of the FEM, using a filament beam element with fibers subjected to a uniaxial stress state, figure 9, Marí [12]. Cracking, yielding, load reversals and the structural effects of the delayed deformations are taken into account, in the structural analysis under loads and imposed deformations. The instantaneous nonlinear behavior of concrete in compression has been considered by means of a parabolic model with a post-peak descending branch and load reversal. A smeared crack approach is used and tension stiffening is considered in the tensile stress-strain branch of concrete. The evolution of concrete mechanical properties due to aging with time have been considered according to the EC2 [13]. For reinforcing steel, a bilinear stress-strain relationship is assumed with load reversals.

Creep strain $\varepsilon cr(t)$ of concrete is evaluated by an age dependent integral formulation based on the principle of superposition. A Dirichlet series is used as creep function, which allows obtaining the creep strain increment at a given instant by a recurrent expression that only requires to store the stress only at the last time step, Bazant [15]. A time step-by-step procedure is performed in which increments of displacements, strains and other structural quantities are successively added
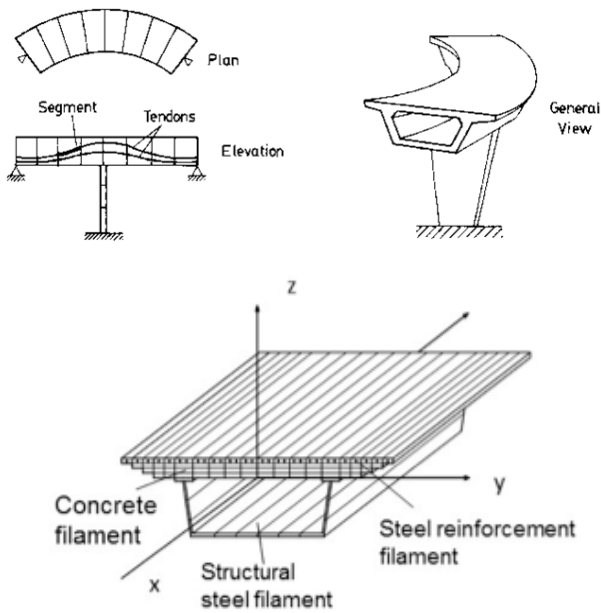
Figure 9. Filamented beam element.

to the previous totals as we march forward in the time domain. At each time step, the structure is analyzed under the external applied loads and under the imposed deformations, such as creep, originated during the previous time interval and geometry. Iterative procedures using load or displacement control, combined with incremental analyses are used to trace the structural response along the structure service life throughout the elastic, cracked and ultimate load levels. For each iteration of each load step and time instant, the following set of non-linear equations is solved:

$$\Delta R = \Delta R^i + \Delta R^{nm} + \Delta R^u = K\delta \tag{1}$$

Where the total load vector ΔR is composed by the vectors due to the internal stresses (ΔR^i), non-mechanical strains, (ΔR^{nm}) and unbalanced forces due to non-linearities (ΔR^u) of the previous iteration, K is the updated stiffness matrix according to the materials state and δ is the vector of nodal displacements. The time-dependent performance of the model was experimentally checked by Marí and Valdés [16], and has been widely used for the non-linear time-dependent analysis of structures including segmentally constructed, deteriorated and strengthened structures Marí et al. [17], Fernández et al. [18].

5.
SIMULATION OF THE STRUCTURAL EFFECTS OF PRESSTRESSING STEEL CORROSION

In the present model, post-tensioning tendons, that can have a straight or parabolic layout, are divided into segments. A segment is the part of the tendon which lies inside an element and is considered straight, and have a constant force see figure 9. When stressing the tendons, the force along the cable varies due to prestressing losses so, at each segment, the force is different. At both ends of each element forces and moments

are generated that give place to the so-called prestressing loads applied at the nodes. Once the tendons are bonded by grouting the ducts, their deformation follow that of the concrete. Then, under applied external loads, the variation of strain at any prestressing segment is obtained calculating the new position of its ends and, therefore the variation of its length. This increment of strain is added to the previous strains, then prestressing stresses are obtained from the constitutive equation of steel, after subtracting the relaxation losses along the elapsed time. The prestressing loads are, then, updated and the new system of non-linear equations is set.

Corrosion of prestressing steel produces a loss of the area of the affected wire, and consequently a loss in the prestressing force, thus resulting in a loss of flexural capacity and stiffness. The loss of steel area due to corrosion is estimated through the following equation:

$$A_p(t) = A_p(t_0)[1 - D_c(t)] \tag{2}$$

Where $A_p(t_0)$ is the initial area of prestressing steel, t is the elapsed time since the initiation of the corrosion and $D_c(t)$ is a function defining the time evolution of the damage:

$$D_c(t) = \left(\frac{t - t_i}{t_f - t_i} \right)^{\beta} \tag{3}$$

Where t_i is the instant of the initiation of the corrosion, t_{fis} is the instant when the steel is totally corroded and $A_p(t_f) = 0$; β is an exponent related to the corrosion rate. For $\beta = 1$, the reduction of steel area is linear, while for $\beta > 1$ and $\beta < 1$ the reduction is faster or slower than linear, respectively. If the corrosion rate, v_{cor}, is known, t_f can be calculated for $\beta = 1$ as:

$$t_f = t_i + \frac{A_p(t_0)}{v_{cor}} \tag{4}$$

The reduced steel area is then adopted by the model, and new internal resisting load vector, prestressing loads and unbalanced load vectors are computed. Then, the iterative procedure, inherent to the non-linear analysis, identifies the lack of equilibrium due to the loss of steel area and prestressing force, and automatically generates the corresponding unbalanced forces to restore equilibrium, Marí et al. [17]

6.
COMPARISON OF TESTS RESULTS AND NUMERICAL SIMULATIONS

The tests previously described have been used to check the capacity of the model to capture the structural effects of prestressing steel corrosion. For this purpose, the tests have been simulated, introducing the same load cycles and the load-deflection curves, were obtained and compared with the experimental ones. It must be remarked that the degree of corrosion of the tendons is not known a priori, so previously to the simulation of the tests, a study devoted to estimate the loss of steel area in order to obtain a similar loss of capacity, was done. The results of such study provided a value of 67,8% loss of steel

area. Then, assuming $\beta = 1$, the final instant $t_f = 6400$ days was derived from Eq. (4) and adopted for the tests simulation.

The beams were idealized by means of 20 equal 1D equal finite elements of 250 mm length, connected by 21 nodes. The cross section was discretized into 100 layers of 2.5 mm thickness. A concrete modulus of elasticity $E_c = 33\,000$ MPa was adopted. Mild steel was simulated as an elastic-plastic material with yield stress $f_y = 4\,200$ MPa. Prestressing steel was considered a bilinear with $f_{py} = 1\,600$ MPa, $f_{pu} = 1\,860$ MPa, $E_p = 195\,000$ MPa and $\varepsilon_{psu} = 0.035$.

After application of the prestressing and self-weight loads at 14 days after casting the beams, a time-dependent analysis was performed during a period of 4 400 days, obtaining the prestressing losses, deflections and redistribution of stresses along the time. Then, a point load was applied at the beam mid-span, following the same loading path than in the tests, up to failure. In the following, the results of the analysis of beams T1, T3 and T4, which correspond to those with bonded tendons and stressed with the maximum allowable prestressing force, are presented.

Figure 10 shows the experimental and numerically obtained load-deflection curves of beam T1, without induced corrosion.
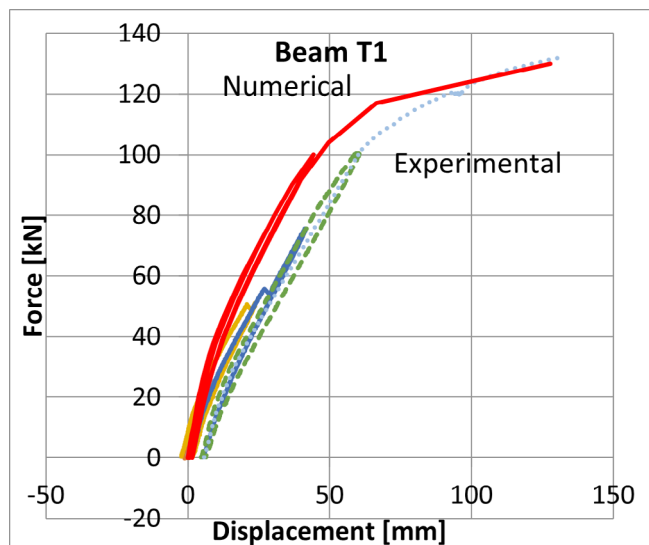

Figure 11. Load-displacement curves, beam T3a.

Figure 10. Load-displacement curves, beamT1

Load control was used in this test, for the six loading and unloading cycles until reaching 25, 50, 75, 100, 130 and 150 kN. The ultimate load found was 130 kN, therefore, only 5 cycles are represented in figure 10. It is observed that the ultimate capacity is very well captured by the numerical model, although the experimentally measured deflections were higher than those numerically obtained.

Beam T3 was corroded in a portion of 1 m length placed at mid-span of the beam. The test was performed under imposed displacements, unloading until zero load was reached, for each cycle. Figure 11 shows the theoretical and the experimentally measured load-deflection curves

It can be observed that the ultimate capacity has been well captured by the numerical model, but there are differences in the shape of the load-displacement curves. The experimental curve shows a lower stiffness and, in addition, a sudden drop of capacity for an imposed displacement of 50 mm,
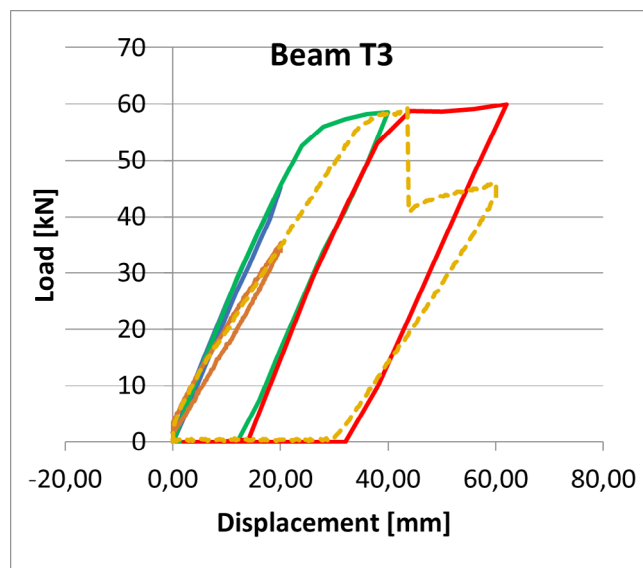
probably due to the break of a wire. Such phenomenon has been not captured by the model, since the constitutive equation of the steel has not been modified as consequence of the corrosion.

Beam T4 was damaged by injecting a chemical solution in a length of 100 mm long, at 1/4 of the length (symmetrically) to cause a localized corrosion of the tendon. The test was performed under displacement control, by means of 6 cycles of 10, 20, 40, 80, 100 and 200 mm, respectively. The ultimate load reached experimentally was 62.3 kN for a displacement of 85 mm, while the numerical model has predicted 64.5 kN for a displacement of 84 mm. Again, the experimental results showed a lower stiffness, although the predictions are quite coincident with the experimental results, as shown in figure 12.
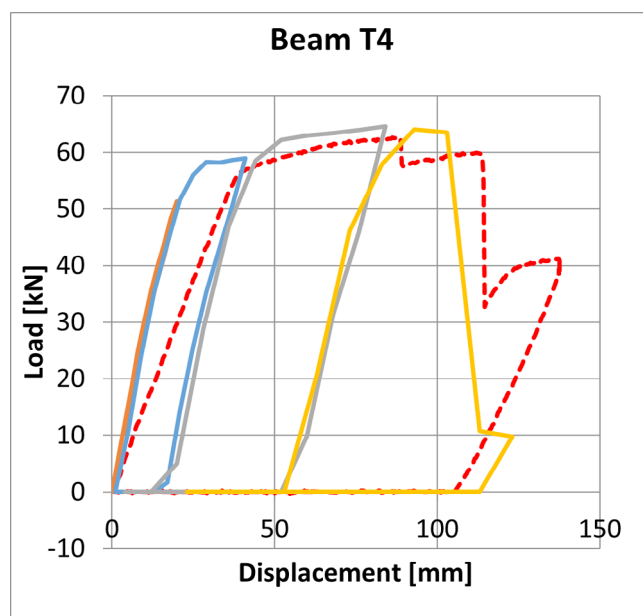

Figure 12. Load-displacement curves, beamT4

7.
CONCLUSIONS

In this work, the experimental results of a group of tests on corroded post-tensioned concrete beams have been presented. The results show that corrosion reduce the load bearing capacity, the stiffness and the displacement at failure of the beam.

In particular, for the tested beams, the reduction of the ultimate load has reached almost 50% with respect to the un-corroded beam. The displacements for the ultimate load were reduced from L/20 for the uncorroded beam to L/42 and L/85 for the corroded beams T3 (corrosion at midspan) and T4 (corrosion at ¼ length), respectively.

During the cycling load tests, a sudden drop of the load bearing capacity have been observed for large displacements, probably due to the rupture of some wires.

In addition, a numerical model for the non-linear and time-dependent analysis of RC and PC structures, previously developed, has been extended to take into account the loss of prestressing steel area and force on the structural response. The model has been used to simulate the tests of the un-corroded and corroded beams, showing very good agreement with the experimental results, especially in terms of load bearing capacity. However, the experimentally measured displacements were bigger than those obtained numerically. In addition, the model did not reproduce the sudden drop of capacity observed in some tests, probably due to the rupture of prestressing wires, thus indicating the need to modify the material properties of the corroded steel.

References

[1] Li, C.Q., Yang, Y. & Melchers R.E. (2008) Prediction of reinforcement corrosion in concrete and its effects on concrete cracking and strength reduction, *ACI Mater.* J. 105: 3–10. https://doi.org/10.14359/19201.

[2] Imperatore, S., Rinaldi, Z. & Drago, C. (2017) Degradation relationships for the mechanical properties of corroded steel rebars, *Constr. Build. Mater.* 148: 219–230. https://doi.org/10.1016/J.CONBUILDMAT.2017.04.209.

[3] Giordano, L., Mancini, G., Tondolo, F. (2009) Numerical Interpretation of Bond Between Steel and Concrete in Presence of Corrosion and Cyclic Action, *Key Eng. Mater.* 417–418: 349–352. https://doi.org/10.4028/www.scientific.net/KEM.417-418.349.

[4] Recupero, A., Spinella, N. & Tondolo, F. (2018) A model for the analysis of ultimate capacity of RC and PC corroded beams, *Adv. Civ. Eng.* https://doi.org/10.1155/2018/8697109.

[5] Nürnberger, U. (2002) Corrosion induced failure mechanisms of prestressing steel, *Mater. Corros.* 53: 591–601. https://doi.org/10.1002/1521-4176(200208)53:8<591::AID-MACO591>3.0.CO;2-X.

[6] Colajanni, P., Recupero, A., Ricciardi, G. & Spinella, N. (2016) Failure by corrosion in PC bridges: A case history of a viaduct in Italy, *Int. J. Struct. Integr.* 7 181–193. https://doi.org/10.1108/IJSI-09-2014-0046.

[7] Prieto, M., Tanner, P. & Andrade, C. (2016) Multiple linear regression model for the assessment of bond strength in corroded and non-corroded steel bars in structural concrete, *Mater. Struct.* 49 4749–4763. https://doi.org/10.1617/s11527-016-0822-8.

[8] Bossio, A., Fabbrocino, F., Monetta, T., Lignola, G.P., Prota, A., Manfredi, G. & Bellucci, F. (2018) Corrosion effects on seismic capacity of reinforced concrete structures, *Corros. Rev.* 37 https://doi.org/10.1515/corrrev-2018-0044.

[9] Colajanni, P., Recupero, A. & Spinella, N. (2019) Push-Over Analysis of RC Frame with Corroded Rebar, *IOP Conf. Ser. Mater. Sci. Eng.* 627 012020. https://doi.org/10.1088/1757-899X/627/1/012020.

[10] Coronelli, D., Castel, A., Vu, N.A. & François, R. (2009) Corroded post-tensioned beams with bonded tendons and wire failure, *Eng. Struct.* 31 1687–1697. https://doi.org/10.1016/J.ENGSTRUCT.2009.02.043.

[11] Castel, A., François, R., Santisi d'Avila, M.P. & Jenkins, D. (2018) New service limit state criteria for chloride in chloride environments, *Corros. Rev.* 0. https://doi.org/10.1515/corrrev-2017-0100.

[12] Marí, A. (1984) Nonlinear Geometric, Material and Time-dependent Analysis of Three Dimensional Reinforced and Prestressed Concrete Frames, *UCB /SESM Report 84/12, University of California, Berkeley.*

[13] Marí, A. (2000) Numerical Simulation of the Segmental construction of Three Dimensional concrete frames. *Eng. Structures*, No. 6, Vol. 22, pp 585-596.

[14] CEN (2003), Eurocode 2: Design of concrete structures - Part 1.1: General rules and rules for buildings.

[15] Bazant ZP, Wittmann FH, (1982). *Creep and shrinkage in concrete structures.* New York: John Wiley and Sons.

[16] Marí, A., Valdés, M. (2000) "Long-Term Behaviour of Continuous Precast Concrete Girder Bridges Model", *ASCE Journal of Bridge Engineering*, No. 1, Vol.5, pp. 22-30,

[17] Marí, A., Mirambell, E., Estrada, I, (2002) "Effects of construction sequence and prestressing of the slab on the service behaviour of composite concrete and steel bridges", Accepted for publication. *Constructional Steel Research Journal* (Elsevier).

[18] Marí, A., Bairán, J., Fernàndez, I. (2011) Modelado numérico de estructuras pretensadas que sufren corrosión bajo tensión. *Final Report, research project SEDUREC (Safety and Durability of Structures and Constructions).* CIMNE, UPC, Barcelona.